

PAPER • OPEN ACCESS

Towards automated ultrasound imaging—robotic image acquisition in liver and prostate for long-term motion monitoring

To cite this article: Svenja Ipsen *et al* 2021 *Phys. Med. Biol.* **66** 094002

View the [article online](#) for updates and enhancements.

You may also like

- [The overrated role of 'promotion' in mechanistic modelling of radiation carcinogenesis](#)
Marco J P Brugmans, Harmen Bijwaard and Henk P Leenhouts
- [Coronal *in vivo* forward-imaging of rat brain morphology with an ultra-small optical coherence tomography fiber probe](#)
Yijing Xie, Tim Bonin, Susanne Löffler et al.
- [Protective ventilation using electrical impedance tomography](#)
H Luepschen, T Meier, M Grossherr et al.



PAPER

OPEN ACCESS




RECEIVED
6 January 2021REVISED
7 March 2021ACCEPTED FOR PUBLICATION
26 March 2021PUBLISHED
23 April 2021

Original content from this work may be used under the terms of the [Creative Commons Attribution 4.0 licence](#).

Any further distribution of this work must maintain attribution to the author(s) and the title of the work, journal citation and DOI.



Towards automated ultrasound imaging—robotic image acquisition in liver and prostate for long-term motion monitoring

Svenja Ipsen^{1,2} , Daniel Wulff¹ , Ivo Kuhlemann¹, Achim Schweikard¹ and Floris Ernst¹ ¹ Institute for Robotics and Cognitive Systems, University of Luebeck, Luebeck, Germany² Fraunhofer Research Institution for Individualized and Cell-Based Medical Engineering IMTE, Luebeck, GermanyE-mail: ernst@rob.uni-luebeck.de**Keywords:** image guidance, sonography, organ motion, motion tracking, robotics, automation

Abstract

Real-time volumetric (4D) ultrasound has shown high potential for diagnostic and therapy guidance tasks. One of the main drawbacks of ultrasound imaging to date is the reliance on manual probe positioning and the resulting user dependence. Robotic assistance could help overcome this issue and facilitate the acquisition of long-term image data to observe dynamic processes *in vivo* over time. The aim of this study is to assess the feasibility of robotic probe manipulation and organ motion quantification during extended imaging sessions. The system consists of a collaborative robot and a 4D ultrasound system providing real-time data access. Five healthy volunteers received liver and prostate scans during free breathing over 30 min. Initial probe placement was performed with real-time remote control with a predefined contact force of 10 N. During scan acquisition, the probe position was continuously adjusted to the body surface motion using impedance control. Ultrasound volumes, the pose of the end-effector and the estimated contact forces were recorded. For motion analysis, one anatomical landmark was manually annotated in a subset of ultrasound frames for each experiment. Probe contact was uninterrupted over the entire scan duration in all ten sessions. Organ drift and imaging artefacts were successfully compensated using remote control. The median contact force along the probe's longitudinal axis was 10.0 N with maximum values of 13.2 and 21.3 N for liver and prostate, respectively. Forces exceeding 11 N only occurred in 0.3% of the time. Probe and landmark motion were more pronounced in the liver, with median interquartile ranges of 1.5 and 9.6 mm, compared to 0.6 and 2.7 mm in the prostate. The results show that robotic ultrasound imaging with dynamic force control can be used for stable, long-term imaging of anatomical regions affected by motion. The system facilitates the acquisition of 4D image data *in vivo* over extended scanning periods for the first time and holds the potential to be used for motion monitoring for therapy guidance as well as diagnostic tasks.

Introduction

Ultrasound imaging offers unique advantages for diagnostic and interventional purposes, such as freedom from ionizing radiation, good soft tissue contrast, high flexibility and real-time image acquisition. Ultrasound is the most commonly used imaging method in the clinic and currently the only modality capable of providing volumetric image data in real-time (referred to as 4D ultrasound). However, the quality of an exam strongly depends on the experience and expertise of the examiner. The manual probe handling required for ultrasound scanning can lead to low reproducibility of the exam and hampers retrospective diagnosis on previously acquired image data due to a missing external frame of reference (Fenster *et al* 2013). Furthermore, the physically straining manual exam makes the acquisition of long-term image data for analysis of dynamic processes over minutes or hours challenging if not impossible (Evans *et al* 2009, Harrison and Harris 2015).

In radiation therapy, ultrasound has shown promise as an image guidance modality for motion compensation between and during therapy fractions (e.g. Boda-Heggemann *et al* 2008, Harris *et al* 2011,

Fast *et al* 2016, Ipsen *et al* 2016). While it has been used for patient setup prior to treatment in many previous studies over the past years (Fontanarosa *et al* 2015), the high level of radiation inside the treatment room during therapy delivery prohibits manual probe handling by the therapy staff. Consequently, the only clinically used ultrasound-based guidance system *Clarity Autoscan* (Elekta, Stockholm, Sweden) is readily available only for prostate monitoring during treatment and currently relies on a static probe holder which is positioned manually prior to treatment and then remains in a fixed position during radiation delivery (Lachaine and Falco 2013, Grimwood *et al* 2018, Han *et al* 2018). Ultrasound imaging with this system is performed using a mechanical 3D probe. An experimental version of this setup has also recently been investigated for the liver where the probe remains in a fixed position and ultrasound imaging is used to confirm the correct target position during breath-hold (Vogel *et al* 2018, Boda-Heggemann *et al* 2019). However, especially the liver and the abdominal body surface are strongly affected by respiratory motion, making maintaining constant probe contact and thus continuous image acquisition challenging.

Robotic probe manipulation could potentially overcome these limitations by replacing the human operator during the probe positioning task. Robotic ultrasound systems have been developed and investigated for different medical applications and tasks, ranging from simple remote-controlled teleoperation to autonomous image acquisition and guidance. In the scope of this work, only similar systems with serial, force-sensitive robotic hardware and a focus on continuous image acquisition *in vivo* will be described here. Thorough overviews of robotic ultrasound systems in the medical field can be found in Priester *et al* (2013), Swerdlow *et al* (2017), Von Haxthausen *et al* (2021).

The teleoperated system proposed by Giuliani *et al* uses a custom robot design with seven degrees of freedom (DoF), an external force sensor and haptic feedback for the operator (Giuliani *et al* 2020). Using standard 2D ultrasound equipment, their system has been tested successfully in 14 patients for remote cardiac ultrasound exams. Several other groups focus on using the commercially available *LBR iiwa 7 R800* (KUKA AG, Augsburg, Germany) with seven DoF and integrated torque measurements for different diagnostic and interventional tasks. Virga *et al* used the *LBR iiwa* for screening the abdominal aorta of five healthy volunteers by sweeping over the target region and continuously acquiring 2D ultrasound images to combine them into a full volume (Virga *et al* 2016). A previously acquired MRI scan is used as a reference for path planning to automate the process. Additionally, the measured contact force was used to compensate tissue deformation in the images caused by the robot in scans of five healthy volunteers (Virga *et al* 2018). Chatelain *et al* developed a control approach to optimize image quality during robotic scan acquisition based on the 2D ultrasound image content (Chatelain *et al* 2017). Automatic probe placement and image quality optimization were demonstrated in an abdominal scan of a healthy volunteer. A similar setup was also used by Esteban *et al* to generate a force-compensated sweep of the spine for interventional needle placement in two patients (Esteban *et al* 2018) and in Tirindelli *et al* (2020) where 2D ultrasound and force data acquired in 19 volunteers were fused to facilitate automatic detection of insertion points for spine injections. Hase *et al* used datasets acquired in 34 healthy volunteers for a deep reinforcement learning approach to control robotic navigation for spinal scans based on the ultrasound image content (Hase *et al* 2020).

Robotic ultrasound systems have also been proposed for motion compensation during image-guided radiotherapy. Schlosser *et al* used a custom-built robot with nine DoF and torque measurements in one axis to hold and move the ultrasound probe on the patient before and during treatment (Schlosser *et al* 2010). While their first prototype was based on a 2D ultrasound system, the second iteration featured a 4D-capable system with an abdominal matrix array probe and online data access (Schlosser *et al* 2016). An optimal probe position for target visualization was calculated prior to scan acquisition based on a previously acquired CT scan. The authors demonstrated the feasibility of their approach in two liver patients by visualizing the therapy targets with the robotic framework and acquiring ultrasound sequences of one to four minutes duration during free breathing with a volumetric frame rate of 3–4 Hz (Schlosser *et al* 2016). The system presented in Şen *et al* (2013), Lediju Bell *et al* (2014) was based on another custom robot design with five DoF and a six-axis force/torque sensor to assist the user with the difficult task of ultrasound probe positioning prior to treatment delivery. Using a mechanical 3D ultrasound probe, the authors investigated the impact of force and position control on reproducibility during probe placement in a canine study of pancreas, liver and prostate (Lediju Bell *et al* 2014). In Lediju Bell *et al* (2016), the group used the developed system for elasticity measurements in abdominal tissue of three healthy volunteers. Their custom design was later replaced by an industrial robotic system with six DoF and integrated torque measurements (Şen *et al* 2016). By combining haptic input provided by the user with information gained from the ultrasound image data, the robot guides the probe towards an optimal position on the patient's body surface. The feasibility of this cooperative control approach was demonstrated in a canine study but so far has not been shown in humans (Şen *et al* 2017). The *LBR iiwa* was used in Seitz *et al* (2020) in an experimental setup to manipulate a 2D ultrasound probe. For probe positioning, the robot was either moved directly to the desired position using hand guidance (i.e. the operator moves the robot by manually exerting

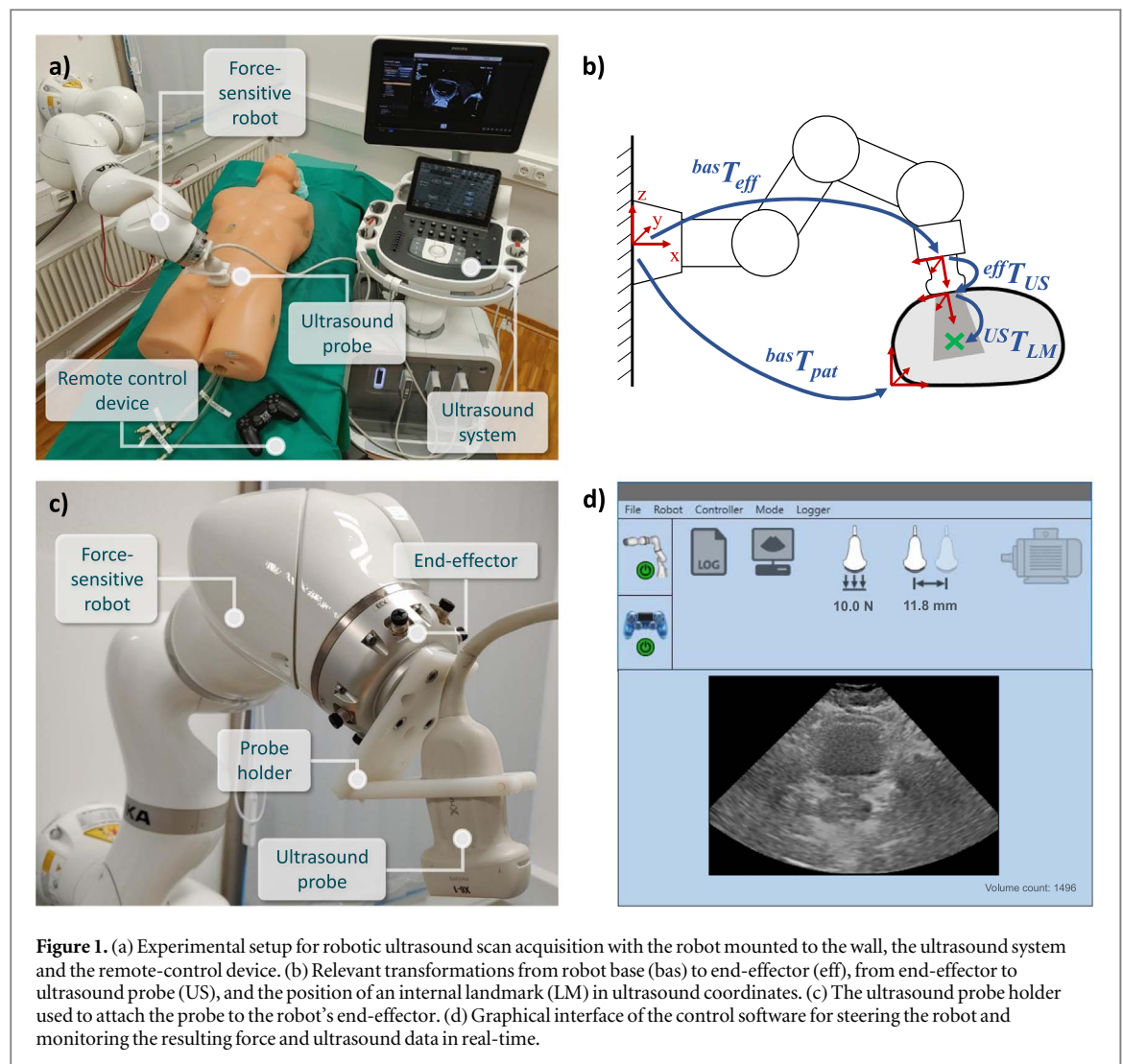


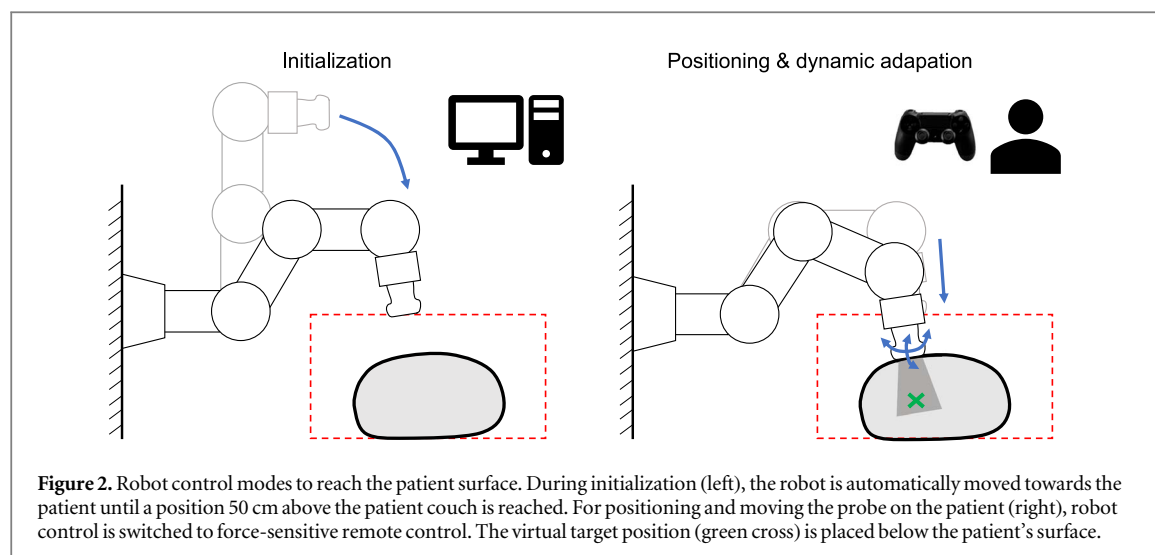
Figure 1. (a) Experimental setup for robotic ultrasound scan acquisition with the robot mounted to the wall, the ultrasound system and the remote-control device. (b) Relevant transformations from robot base (bas) to end-effector (eff), from end-effector to ultrasound probe (US), and the position of an internal landmark (LM) in ultrasound coordinates. (c) The ultrasound probe holder used to attach the probe to the robot's end-effector. (d) Graphical interface of the control software for steering the robot and monitoring the resulting force and ultrasound data in real-time.

external force on the joints) or via remote control. Feasibility was demonstrated in two healthy volunteers by acquiring ultrasound sequences of the liver for a duration of two minutes.

Most *in vivo* experiments with robotic ultrasound systems have been limited to the use of 2D ultrasound imaging, a small number of subjects and short scan times of less than four minutes. However, most therapeutic interventions require much longer treatment times, for example high-dose stereotactic body radiotherapy (SBRT) which can require up to 30–60 min for dose delivery while at the same time posing the highest demands on accuracy and thus image guidance due to the steep dose gradients. Longer observation times would not only be more representative of SBRT treatments but could also provide valuable insights into the dynamic patterns of internal target motion. Publicly available ultrasound datasets of the liver used for tracking studies were acquired manually and are thus also limited to short scan times (De Luca *et al* 2015, 2018). Due to the lack of information about probe position or motion during scan acquisition, it would also be difficult to retrospectively investigate the absolute target motion extent based on these datasets. At the same time, the technical challenges of robotic long-term ultrasound scanning and its stability over time have not been investigated to date. It is yet unclear how image quality changes over the course of a prolonged imaging session and if a single application of ultrasound gel at the start of the scanning procedure is sufficient for continuous image acquisition. It has also not been investigated how often manual intervention via remote control is needed and if typical movements of the scanned subjects lead to system failures.

Our previous studies on robotic ultrasound focused on the development of an inverse kinematic model for the seven-DoF *LBR iiwa* (Kuhlemann *et al* 2016) and the integration of this robot into the radiotherapy workflow through camera-based patient registration (Kuhlemann *et al* 2015). At the same time, we demonstrated that 4D ultrasound imaging can be used for motion monitoring and online treatment adaptation during radiotherapy (Ipsen *et al* 2016, 2017) using high-accuracy probe calibration and real-time visualization (Ipsen *et al* 2018).

The aim of this study was to combine both areas—robotics and 4D ultrasound imaging—to assess the feasibility of performing stable, long-term image acquisition using robotic automation with active motion



compensation and remote probe steering. For this purpose, a robotic ultrasound system was developed to acquire 4D image data over extended scan periods of 30 min or more. To cover a range of force profiles and motion patterns, five subjects were scanned in two anatomical regions specifically suited for ultrasound-based image guidance: prostate and liver. The primary aspects investigated in this study were (I) Quantification of the system's performance regarding image acquisition and motion compensation during extended scan sessions, and (II) Feasibility to characterize target motion for the investigated anatomical regions. For future studies on motion monitoring in ultrasound images, the data generated in this study (including robot motion, estimated forces, ultrasound volumes and landmark annotations) can be made available upon request.

Materials and methods

Robotic automation of ultrasound imaging requires the integration of its central components—robot, ultrasound hardware, control software—into one system to ensure safe operation as well as stable performance for long-term image acquisition. The complete system was then assessed in a volunteer study regarding stability, dynamic probe repositioning and continuity of image acquisition.

Experimental setup

The setup consists of a serial robotic arm, an ultrasound station and a control computer, shown in figure 1(a). An *EPIQ7* ultrasound system (Philips Healthcare, Best, Netherlands) was used with an abdominal X6-1 matrix array probe capable of acquiring volumetric image data in real-time (referred to as 4D ultrasound). The 4D data was transferred to the control computer via Ethernet using a proprietary streaming interface provided by the manufacturer and stored for retrospective analysis. Volume size, and thus the resulting acquisition frame rate, was chosen for each scan session based on the individual anatomy.

A light-weight robotic arm (*LBR iiwa 7 R800*; KUKA) was used to manipulate the probe. This robot with seven DoF provides integrated torque measurements in each joint which can be used to estimate forces and has a maximum reach of 800 mm from its base. Figure 1(b) illustrates the different coordinate systems and transformations involved. The robot's base was mounted on the wall next to the patient couch and the position of the robot relative to the patient ${}^{bas}T_{pat}$ was approximated based on this fixed arrangement. The position and orientation of the robot's end-effector relative to its base ${}^{bas}T_{eff}$ was continuously measured during the experiment. The ultrasound probe was rigidly connected to the robot's end-effector using a custom probe holder, shown in figure 1(c), manufactured based on the probe dimensions. Using the mechanical construction parameters of the probe holder, the fixed coordinate transformation ${}^{eff}T_{US}$ from robot to ultrasound coordinates was estimated prior to data acquisition. The position of an internal landmark was determined manually in the ultrasound volumes (see also section 2.4).

Robot and ultrasound system were connected to the control computer via Ethernet. A control software with a graphical user interface, shown in figure 1(d), was implemented to support the operator in monitoring the current robot position and estimated force at the end-effector as well as the ultrasound images in real time. The current pose of the robot's end-effector ${}^{bas}T_{eff}$, the torque values for each joint as well as the resulting force calculated at the end-effector were recorded on the control computer in a log file at a sampling frequency of 200 Hz with corresponding time stamps.

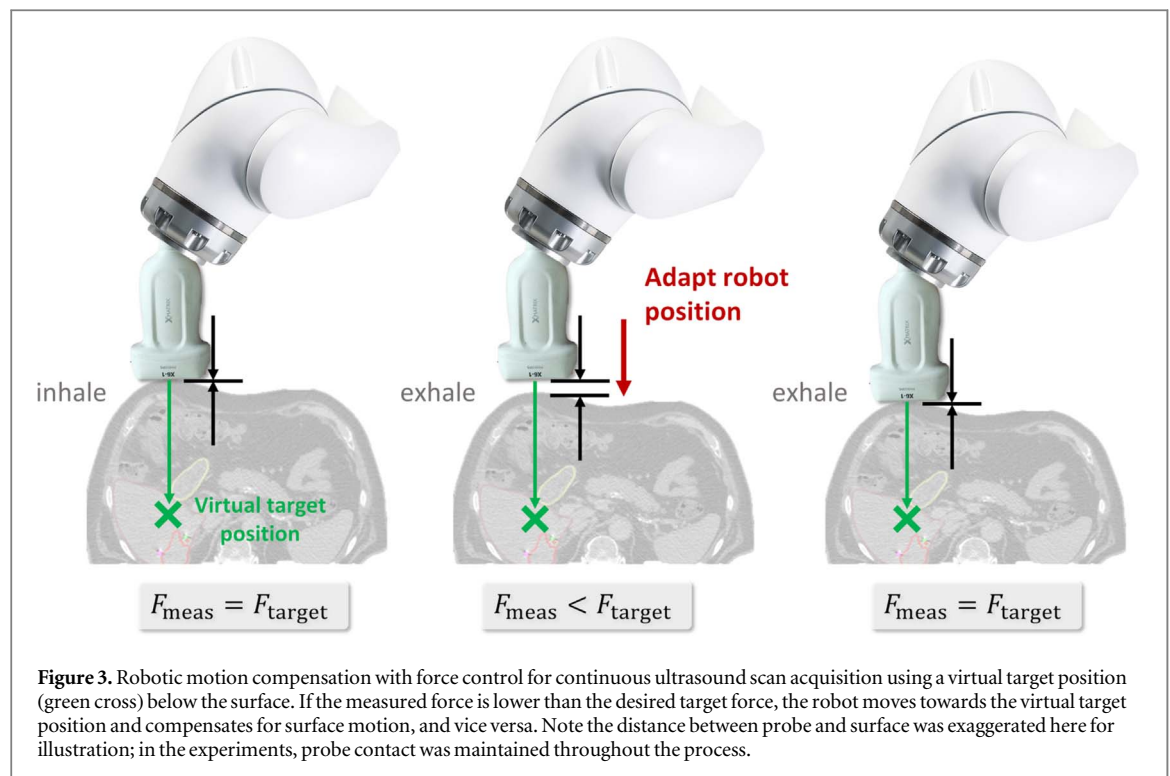


Figure 3. Robotic motion compensation with force control for continuous ultrasound scan acquisition using a virtual target position (green cross) below the surface. If the measured force is lower than the desired target force, the robot moves towards the virtual target position and compensates for surface motion, and vice versa. Note the distance between probe and surface was exaggerated here for illustration; in the experiments, probe contact was maintained throughout the process.

Robotic scan acquisition

As illustrated in figure 2, robot motion was divided into an automatic and a manual control phase based on the distance from the patient couch. An inverse kinematics algorithm for robots with seven DoF was used for both control modes (Kuhlemann *et al* 2016). The additional seventh DoF was exploited to optimize the kinematic pose regarding joint range limitations during operation as well as to maximize the distance of the robot's elbow from the patient for safety.

First, the robot was moved in automatic mode to a position 50 cm above the couch surface. Collision detection was enabled to ensure patient and operator safety during this initial approach. If a collision was detected, the robot performed a safety stop to avoid injury. Within the higher-risk area closer to the patient (distance <50 cm), robot control was switched to manual remote control. A conventional controller with two joysticks (see figure 1) was used to command slow translational and rotational motion of the ultrasound probe, respectively, to approach the patient and identify the anatomical target region within the ultrasound images.

Since ultrasound imaging requires surface contact between the probe and the patient, it is necessary to compensate for motion during scan acquisition. This compensation can be achieved by measuring and adapting the current contact force. To realize the desired force-compensated, remote-controlled robot motion, a custom control mode was implemented, combining the robot's real-time position control of the fast research interface for motion commands with a force compensation software module provided by the manufacturer. The compliant mode relies on Cartesian impedance control with a spring-damper model where the spring constant k (in N m^{-1}) determines the robot's stiffness in three axes. For the purpose of robotic probe placement, spring constants were set to $k_z = 0 \text{ N m}^{-1}$, $k_x = 100 \text{ N m}^{-1}$, $k_y = 100 \text{ N m}^{-1}$. As a result, forces in z -direction (along the longitudinal probe axis), being the main direction of superficial breathing motion, would be compensated fast with low stiffness. Lateral motion compensation on the other hand would be less compliant and therefore occur to a lesser degree, mainly to avoid loss of target visibility. The desired target force along the main probe direction was defined as $F_{\text{target}} = 10 \text{ N}$ to generate continuous, high-quality ultrasound images. These values were chosen empirically based on previous experiments to achieve robust robotic motion compensation while holding the probe at the desired location for ultrasound scan acquisition without causing pain or discomfort. A force threshold of $F_{\text{thresh}} = 25 \text{ N}$ was defined as a stopping criterion for the experiments to ensure patient safety and comfort.

During remote control, the robot's joint torques were continuously monitored and used to estimate the contact force at the end-effector based on internal calculations provided by the manufacturer. The robot would move to a commanded position while the condition $F_{\text{meas}}(t) \leq F_{\text{target}}$ was fulfilled. If $F_{\text{meas}}(t) > F_{\text{target}}$, the robot would not move further but instead compensate the increasing force by moving in the opposite direction (see figure 3). Once the operator determined a suitable probe position and orientation for image acquisition, a virtual target point was defined for the robot along the z -direction away from the probe and below the patient's surface.



Figure 4. Experimental setup and probe placement for intercostal liver (top) and transabdominal prostate scans (bottom).

Since this point cannot be reached without exceeding F_{target} , the probe remained at its current location while continuously compensating for patient motion as illustrated in figure 3. This method for remote control also allows changing the probe position during scan acquisition, for example to readjust the field of view due to target motion.

Volunteer study protocol

To assess the performance of the developed system regarding long-term image acquisition and motion compensation, an *in vivo* feasibility study was conducted. The study protocol was approved by the Ethics Committee at the University Clinic Schleswig-Holstein (reference number 18-219). In the scope of this initial feasibility study, five male healthy volunteers (age 27–38 years) were included to receive ultrasound scans of the liver and the prostate for a duration of 30 min, respectively (ten scan sessions total).

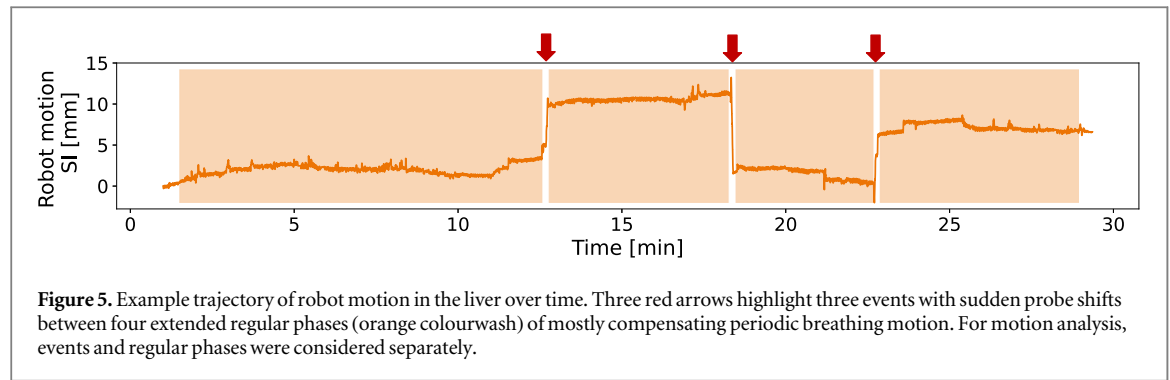
During the first session, ultrasound images were acquired of the liver through an intercostal acoustic window (see figure 4) during free breathing. No specific breathing instructions were given. For the second session, the volunteers were asked to empty their bladders and then drink two litres of water immediately before the experiment to investigate the magnitude and dynamic behaviour of prostate motion caused by rapid and pronounced bladder filling. Scans of the prostate were acquired with a transabdominal (suprapubic) probe position (see figure 4).

The operator conducting the experiments with the developed system was an expert user of the *LBR iiwa* robot with additional experience in 4D ultrasound imaging. The operator was responsible for placing the probe on the patient and reaching an imaging position with good target visibility and image quality. During scan acquisition, the operator monitored the ultrasound images continuously and determined qualitatively if manual repositioning was required. For both anatomical regions, ultrasound gel was applied at the intended probe position in the beginning of the scan session. If a loss of coupling was observed during scan acquisition, the probe would be lifted manually via remote control to renew the gel layer.

Data evaluation

The goal of this study was to investigate two major aspects of robotic ultrasound and its use for motion monitoring during extended scan sessions: (I) system performance regarding image acquisition and motion compensation, and (II) feasibility to quantify target motion in the acquired ultrasound image data.

Ultrasound volumes, robot motion and force data were acquired simultaneously over the entire scan duration of 30 min. Due to separate clocks used by the robot and the ultrasound system, the respective data points first had to be synchronized retrospectively. Based on its characteristic appearance in both data sets, the event of reaching surface contact was selected for synchronization. In the robot data, this was represented by a



strong increase in the measured force signal. In the ultrasound images, a transition from sensor noise to anatomical content could be measured by calculating their entropy and identifying a strong increase.

Robotic system performance

The scan sessions were analysed regarding system stability, adaptability of the probe position via remote control, continuity in image acquisition and image quality as well as patient comfort.

System stability was assessed qualitatively based on the occurrence of technical interruptions during image acquisition and quantitatively by measuring the accuracy and precision of the utilized force control approach. The estimated force values were evaluated regarding their magnitude and distribution over time and compared to the desired value F_{target} .

For quantitative characterization of the probe motion, the robot data was analysed with respect to motion extent and variability. Probe motion was often comprised of stable phases interrupted by distinct events with sudden, pronounced probe motion and concomitant force peaks. An example probe motion trajectory in the liver with three distinct events is illustrated in figure 5. Motion statistics were calculated separately for the regular phases and the intermediate probe shifts. The initial probe positioning process at the beginning of the experiment and the probe removal at the end were excluded from the motion analysis to maintain a focus on typical patient motion and robotic motion compensation.

To evaluate the continuity of ultrasound image acquisition and changes in image quality over time, the entropy of each ultrasound volume was calculated (Kuhlemann *et al* 2014). For comparability, the resulting values were normalized for each scan session. High entropy values indicate structured anatomical image content in the ultrasound data while low entropy values are expected for empty volumes containing only sensor noise and for volumes with lower image quality affected by shadowing artefacts from bones or air.

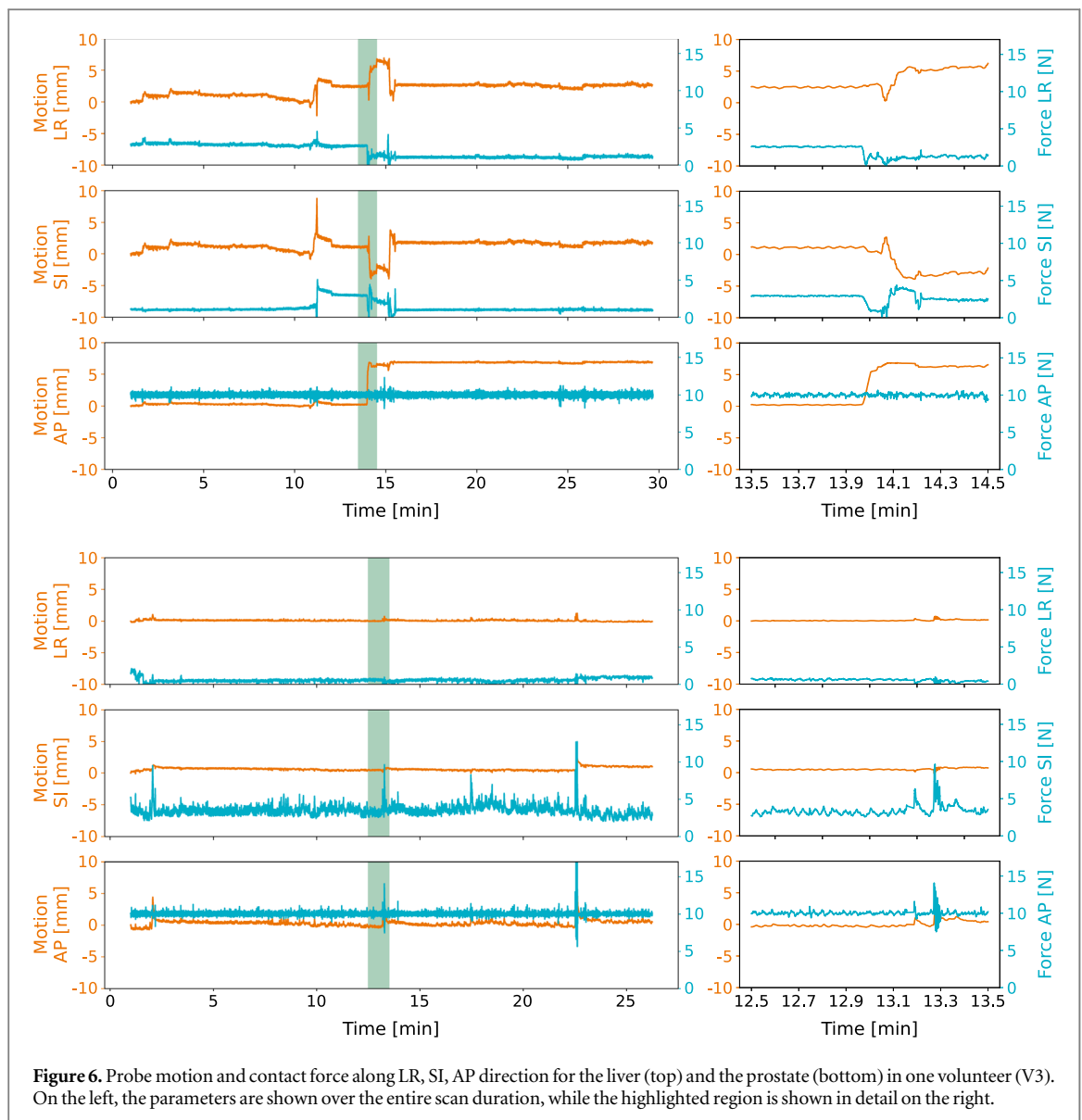
Additionally, the volunteers were asked to score their scanning experience based on two statements: (Q1) ‘I felt no pain during the scan’ and (Q2) ‘I felt no discomfort during the scan’, using a scoring system from 0 to 4 (0—strongly disagree, 1—disagree, 2—neutral, 3—agree, 4—strongly agree) (Wang *et al* 2019).

Internal target motion

To assess the feasibility of measuring internal target motion with long-term robotic ultrasound, a relevant target structure was defined in each ultrasound data set—a liver vessel bifurcation with good visibility or the centroid of the prostate. The selected landmark was annotated manually by an expert trained in 4D ultrasound image interpretation. To visualize long-term trends, the landmark was annotated in 10 s intervals over the entire scan time for each dataset. Additionally, the landmark was annotated in every second frame in two sections with a duration of 30 s each, first after 7 min and second after 22 min, to highlight short-term motion pattern characteristics. This resulted in 273–337 landmarks per scan session (3056 landmarks in total). The external probe motion recorded by the robot ${}^{bas}T_{eff,i}$ and the internal motion of the landmark ${}^{US}T_{LM,i}$ were combined and transformed into the robot base coordinate system

$${}^{bas}T_{LM,i} = {}^{bas}T_{eff,i} {}^{eff}T_{US} {}^{US}T_{LM,i}$$

to perform the motion analysis in a static frame of reference. Target motion statistics such as maximum motion extent and interquartile motion range were then assessed for all datasets, again differentiating between phases of regular motion and irregular events.



Results

Robotic ultrasound scans were successfully acquired in all five volunteers for the target regions in liver and prostate. Probe contact was initialized via remote control and was maintained continuously over each scan session.

Robotic system performance

Robotic probe manipulation with dynamic motion compensation through force control facilitated continuous 4D ultrasound image acquisition without interruptions in all experiments. No technical failures of the robotic system were observed. Using force-compensated remote control, the probe position on the body surface could be readjusted during scan acquisition after the initial probe placement.

While probe motion trajectories and force values, illustrated in figure 6, followed regular patterns compensating the periodic breathing motion most of the time, distinct events with sudden motion of the ultrasound probe or peaking force values were also observed, leading to manual interventions via remote control. As shown in table 1, manual interventions occurred for scans of the liver in four out of five experiments, with two volunteers requiring three readjustments and two requiring two. The prostate scans did not require manual intervention to correct the probe position. The liver's higher mobility, for example caused by changing breathing patterns or coughing, likely led to this higher number of instances where target visibility had to be restored manually by the operator.

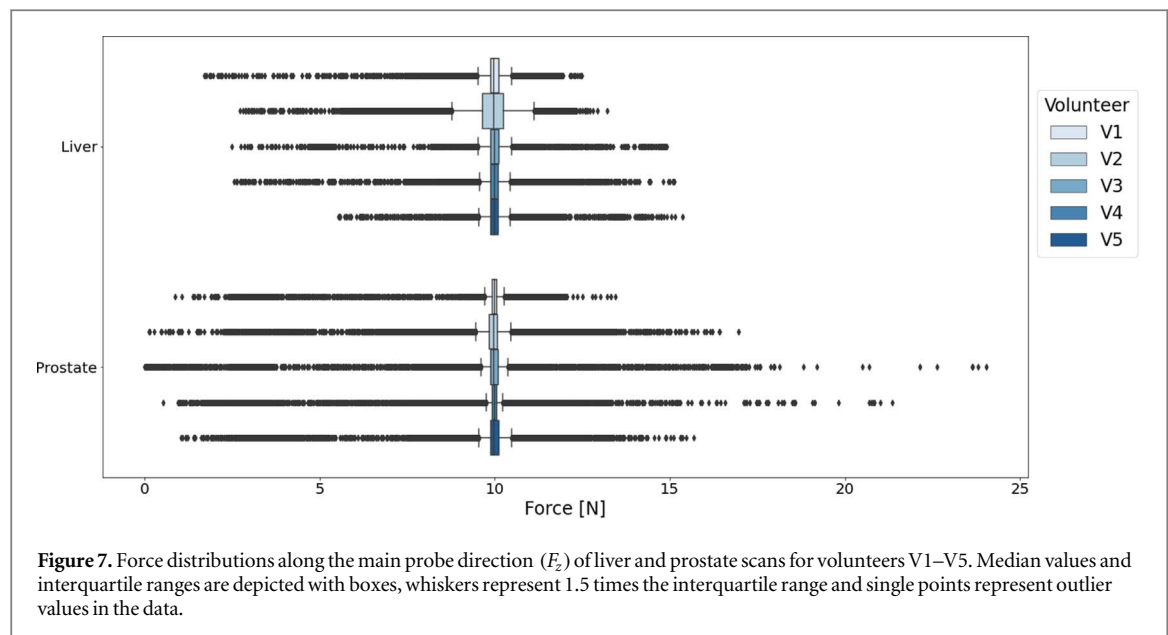


Figure 7. Force distributions along the main probe direction (F_z) of liver and prostate scans for volunteers V1–V5. Median values and interquartile ranges are depicted with boxes, whiskers represent 1.5 times the interquartile range and single points represent outlier values in the data.

Table 1. Number of remote-control events (n_{RC}), median force, interquartile range and maximum force along the main probe direction (F_z) in liver and prostate for volunteers V1–V5 (in N).

	Liver					Prostate				
	V1	V2	V3	V4	V5	V1	V2	V3	V4	V5
n_{RC}	3	3	2	2	—	—	—	—	—	—
$F_{z, Median}$	10.0	10.0	10.0	10.0	10.0	10.0	10.0	10.0	10.0	10.0
$F_{z, 25\%}$	9.9	9.7	9.9	9.9	9.9	9.9	9.8	9.9	9.9	9.9
$F_{z, 75\%}$	10.1	10.2	10.1	10.1	10.1	10.1	10.1	10.1	10.1	10.1
$F_{z, Max}$	11.7	13.2	12.3	13.0	12.1	13.4	16.7	18.0	21.3	15.7

Force control

Contact force distributions and corresponding statistical parameters are summarized in table 1. Over all scan sessions, the median estimated contact force F_z in the main direction of motion compensation, i.e. along the longitudinal probe axis, was 10.0 N with an interquartile range of 9.9–10.1 N. For 90% of the time, the contact force F_z was between 9.6 and 10.4 N. Median lateral forces were lower and ranged from 0.5 to 3.5 N.

Figure 7 shows that the distributions of contact force varied only slightly between subjects. Differences were mainly observed in the outlier values. While irregular events with abrupt probe motion were successfully compensated in real-time during scanning, these events caused short, steep increases in contact force. As a result, maximum force values of 11.7–13.2 N were observed in the five liver scans. In the prostate, the maximum forces were higher, ranging from 13.4 to 21.3 N between subjects. However, forces exceeding the target force by more than 10% were only observed in short, distinct peaks in 0.2% and 0.3% of the time for liver and prostate, respectively.

Probe motion

The amount of robotic probe motion observed during ultrasound scan acquisition, described by the maximum motion extent between the minimum and maximum probe position and the interquartile range, is summarized in table 2. Probe motion patterns differed between anatomical regions as well as between scanned subjects, with one example shown in figure 6.

For scans acquired in the liver through an intercostal viewport, probe motion was more pronounced. During the regular motion phases, i.e. excluding abrupt probe shifts, the maximum motion magnitude was between 5.8 and 12.1 mm for all five volunteers, with interquartile ranges from 0.5 to 2.1 mm. The main direction of probe motion was in superior–inferior (SI) and left–right (LR) direction of the scanned subject, corresponding to the y - and x -axes in robot base coordinates. The smallest amount of probe motion was observed in anterior–posterior (AP) direction (z -axis). This directionality is in agreement with the experimental setup since the probe was placed in a lateral position to reach an intercostal viewport (see figure 4). Four out of five liver scans contained two to three distinct events with sudden probe shifts from remote control events to regain or improve target

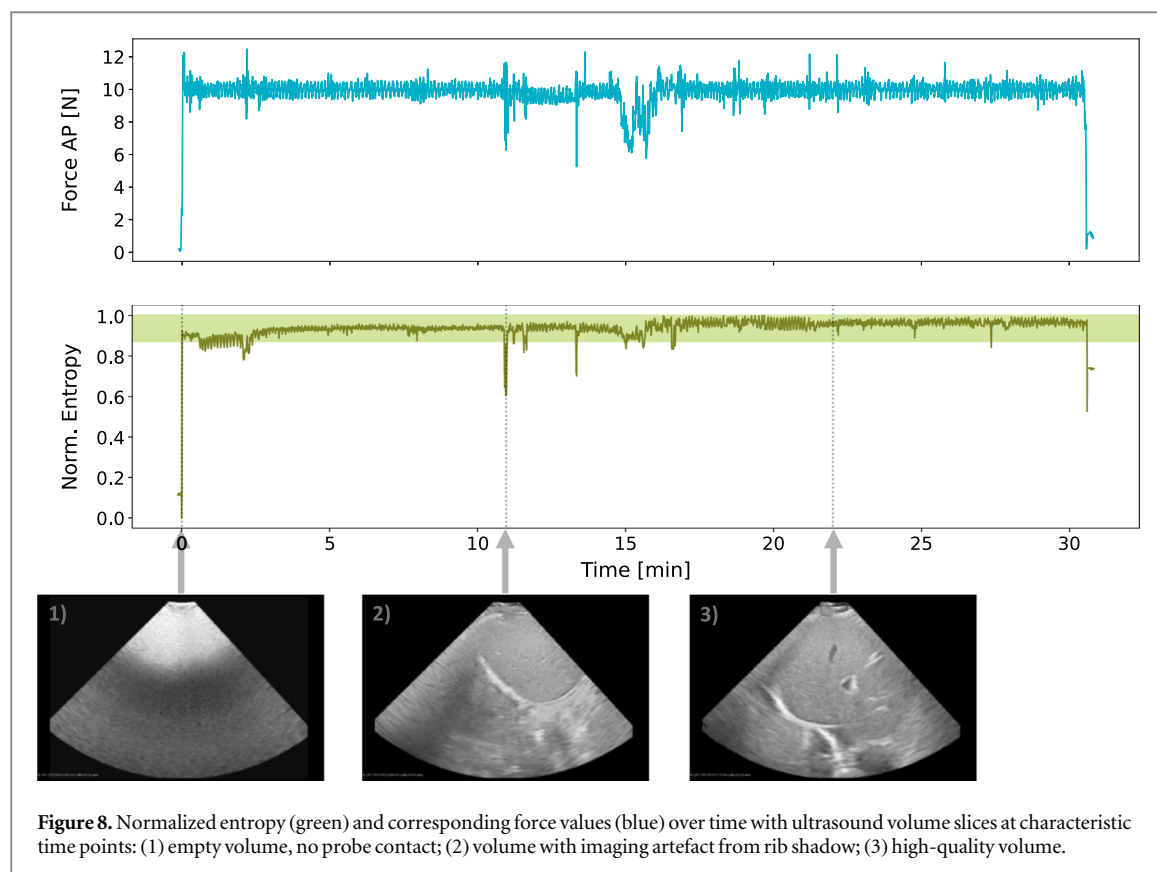


Table 2. External probe and internal landmark motion in liver and prostate for volunteers V1–V5 with maximum 3D motion extent between minimum and maximum position ($\Delta_{\text{Min}, \text{Max}}$), interquartile range ($\Delta_{25\%, 75\%}$), drift of the landmarks between scan start and end (Δ_{drift}) and the percentage of excursions over 3 mm / 5 mm relative to the starting position ($p_{>3 \text{ mm}}$, $p_{>5 \text{ mm}}$).

		Liver					Prostate				
		V1	V2	V3	V4	V5	V1	V2	V3	V4	V5
External probe motion:											
$\Delta_{\text{Min}, \text{Max}}^{\text{probe}}$ (mm)	LR	3.9	5.9	7.4	6.2	3.9	0.8	1.0	1.4	1.6	1.3
	SI	5.4	10.1	9.6	8.5	4.1	1.0	5.2	3.1	4.5	4.0
	AP	1.0	1.6	1.4	1.7	1.2	2.3	12.9	7.0	10.1	8.8
	3D	6.8	11.7	12.1	10.6	5.8	2.6	13.9	7.8	11.2	9.7
$\Delta_{25\%, 75\%}^{\text{probe}}$ (mm)	LR	0.7	1.0	0.3	0.6	0.9	0.1	0.2	0.1	0.1	0.3
	SI	0.7	1.5	0.3	2.0	1.1	0.1	1.6	0.3	0.4	0.5
	AP	0.2	0.2	0.1	0.3	0.2	0.3	3.8	0.5	0.4	0.7
	3D	1.0	1.9	0.5	2.1	1.5	0.3	4.1	0.6	0.6	0.9
Internal landmark motion:											
$\Delta_{\text{Min}, \text{Max}}^{\text{LM}}$ (mm)	LR	5.2	11.6	5.9	7.5	10.8	9.8	13.6	11.3	11.1	4.7
	SI	24.1	41.1	20.7	28.8	37.1	8.2	11.8	4.4	6.2	8.3
	AP	9.5	14.3	10.3	11.2	23.6	3.4	15.7	7.3	10.5	4.8
	3D	26.4	45.1	23.9	31.8	45.2	13.2	23.9	14.2	16.5	10.7
$\Delta_{25\%, 75\%}^{\text{LM}}$ (mm)	LR	1.1	5.1	1.2	1.2	2.3	1.1	2.1	2.7	0.8	1.5
	SI	3.9	18.3	4.9	8.9	13.0	1.5	2.0	1.1	1.2	1.6
	AP	1.6	4.7	2.4	3.4	8.8	0.9	3.7	1.6	1.1	1.6
	3D	4.3	19.6	5.6	9.6	15.8	2.1	4.7	3.3	1.8	2.7
$\Delta_{\text{drift}}^{\text{LM}}$ (mm)	LR	−0.9	4.0	1.1	4.3	0.5	2.3	5.3	8.7	−3.6	1.6
	SI	2.4	2.5	1.5	−5.5	4.1	2.2	−2.5	0.7	2.3	3.4
	AP	−0.3	−0.6	5.2	0.8	0.0	−0.4	7.2	4.7	−0.9	0.8
	3D	2.5	4.7	5.6	7.0	4.1	3.2	9.3	9.9	4.4	3.8
$p_{>3 \text{ mm}}^{\text{LM}}$ (%)		79.9	90.6	82.9	97.0	93.3	66.4	48.1	93.4	11.1	43.4
$p_{>5 \text{ mm}}^{\text{LM}}$ (%)		48.2	74.3	68.2	85.5	82.8	13.8	12.8	71.7	2.9	1.2

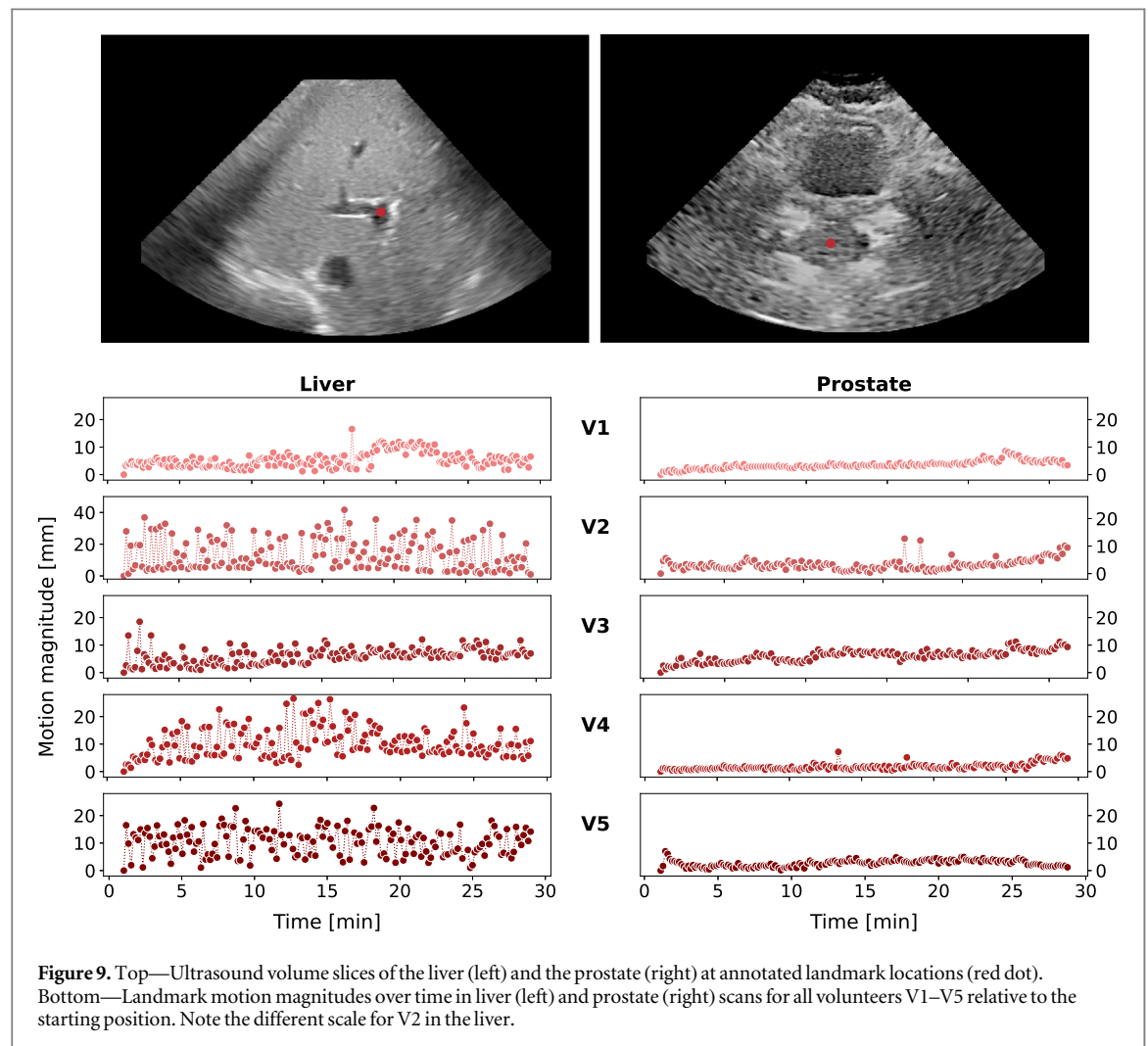
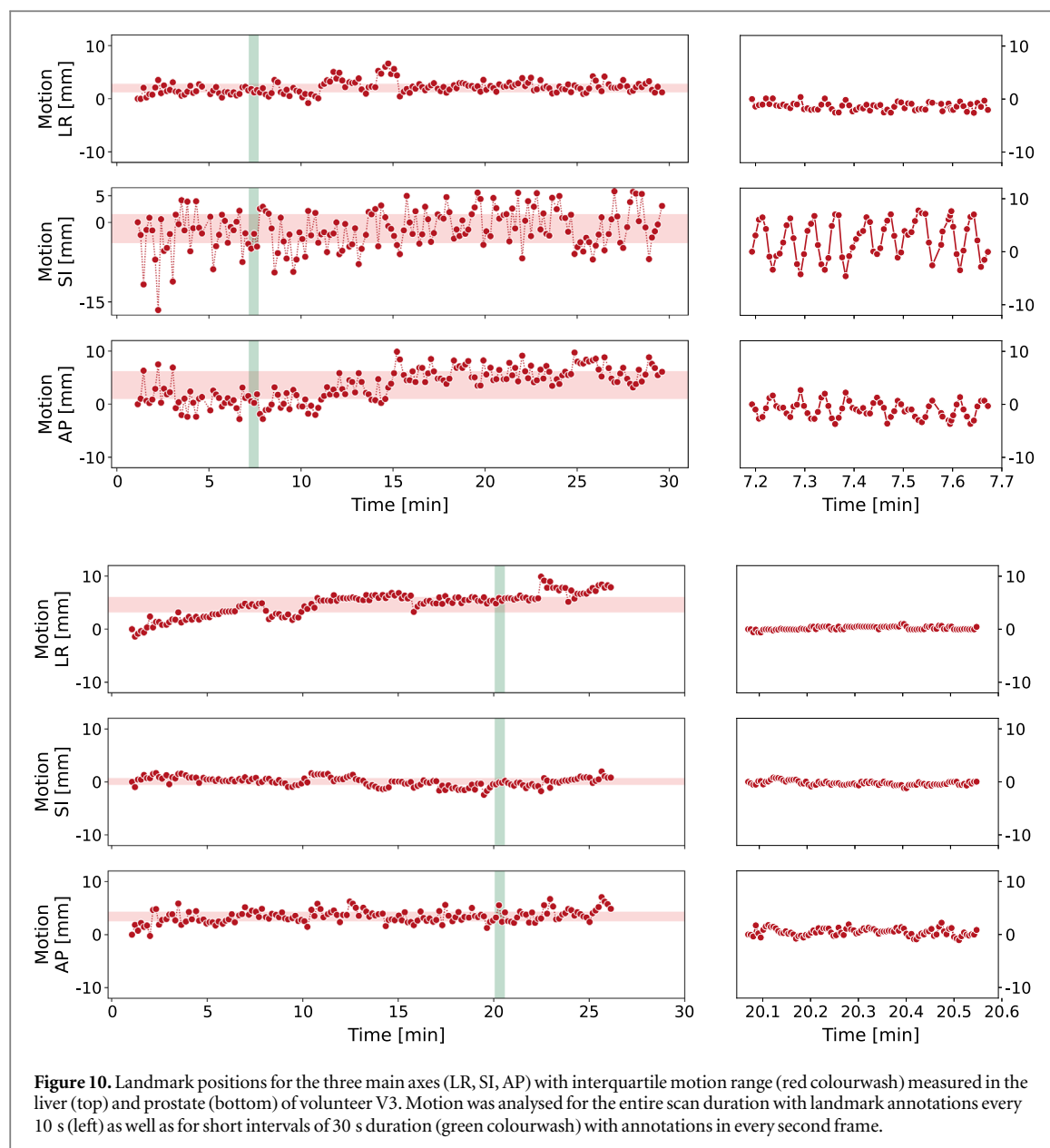


Figure 9. Top—Ultrasound volume slices of the liver (left) and the prostate (right) at annotated landmark locations (red dot). Bottom—Landmark motion magnitudes over time in liver (left) and prostate (right) scans for all volunteers V1–V5 relative to the starting position. Note the different scale for V2 in the liver.

Table 3. Overview of the ultrasound datasets generated in this study. Five volunteers received robotic ultrasound scans of liver and prostate. Landmarks were annotated manually (one per frame) in a subset of the total number of frames.

Organ	Subject	Volumetric framerate (Hz)	Scan duration (min:s)	Sector size	Volume size (mm ³)	Voxel spacing (mm ³)	No. of annotated frames
Liver	V1	4.0	31:10	91° × 60°	240 × 246 × 126	1.0 × 0.7 × 1.4	321
	V2	3.5	30:30	88° × 60°	256 × 260 × 133	1.1 × 0.8 × 1.6	279
	V3	4.5	31:30	90° × 55°	240 × 245 × 117	1.0 × 0.7 × 1.4	308
	V4	3.5	30:10	88° × 60°	256 × 260 × 133	1.1 × 0.8 × 1.6	276
	V5	3.8	30:20	88° × 60°	256 × 252 × 129	1.0 × 0.7 × 1.5	273
Prostate	V1	5.4	27:30	88° × 60°	224 × 228 × 118	0.8 × 0.5 × 1.1	316
	V2	4.7	29:00	88° × 59°	224 × 237 × 122	0.9 × 0.6 × 1.2	299
	V3	6.0	28:00	88° × 55°	224 × 228 × 110	1.0 × 0.7 × 1.4	337
	V4	4.7	30:50	88° × 58°	224 × 237 × 122	0.9 × 0.6 × 1.2	324
	V5	5.0	30:10	88° × 55°	224 × 236 × 114	0.9 × 0.6 × 1.2	323

visibility in the ultrasound images, for example due to coughing or position adjustments by the patient. On average, the magnitude of these shifts was 6.6 mm, ranging from 4.6 to 10.1 mm. The prostate scans, acquired through a transabdominal viewport, showed maximum probe motion magnitudes between 2.6 and 13.9 mm. In all experiments, the main direction of probe motion was in AP (z-axis), as can be expected for the medial probe position chosen for scan acquisition (see figure 4). Interquartile motion ranges were typically lower compared to the liver, laying between 0.3 and 0.9 mm, with the exception of volunteer V2, who had a motion range of 4.1 mm.



Ultrasound image acquisition

4D ultrasound image data was successfully acquired for 30 min in all ten experiments. In all cases, a single application of ultrasound gel was sufficient for image acquisition over the entire scan duration. In the liver, the mean Cartesian volume and voxel sizes were $250 \times 253 \times 128 \text{ mm}^3$ and $1.0 \times 0.7 \times 1.5 \text{ mm}^3$, respectively, with a mean volumetric acquisition rate of 3.9 Hz (range 3.5–4.5 Hz). With a mean sector size of 89° in lateral and 59° in elevational direction and an imaging depth of 25.3 cm, the volumes covered much of the organ with a wide field of view. For the prostate scans, mean volume and voxel sizes were slightly smaller ($224 \times 233 \times 117 \text{ mm}^3$, $0.9 \times 0.6 \times 1.2 \text{ mm}^3$) due to the smaller target region, with a mean volumetric acquisition rate of 5.1 Hz (range 4.7–6.0 Hz) and sector sizes of 88° by 57° at 23.3 cm depth. Scan parameters for all sessions can be found in table 3.

Defining entropy as image quality measure, figure 8 shows a typical course of entropy values and the corresponding force values over time. A steep increase of the entropy was observed at scan initialization for all experiments, indicating the transition from empty, noise-dominated volumes when the probe is still in the air to volumes containing anatomical information when probe contact was established and contact force increased accordingly. For the remainder of the scan, the normalized entropy values generally remained high and narrowly distributed (0.96 ± 0.01 ; mean \pm standard deviation), demonstrating continuous acquisition of ultrasound volumes without loss of contact using the robotic setup. The entropy also showed a correlation with contact force values over time ($R^2 = 0.67$). The mean correlation coefficient was higher in the liver ($R^2 = 0.76$) compared to the prostate ($R^2 = 0.59$). Additionally, short but distinct decreases in entropy values were observed in the liver scans of all subjects. Visual inspection of the corresponding ultrasound volumes showed the presence

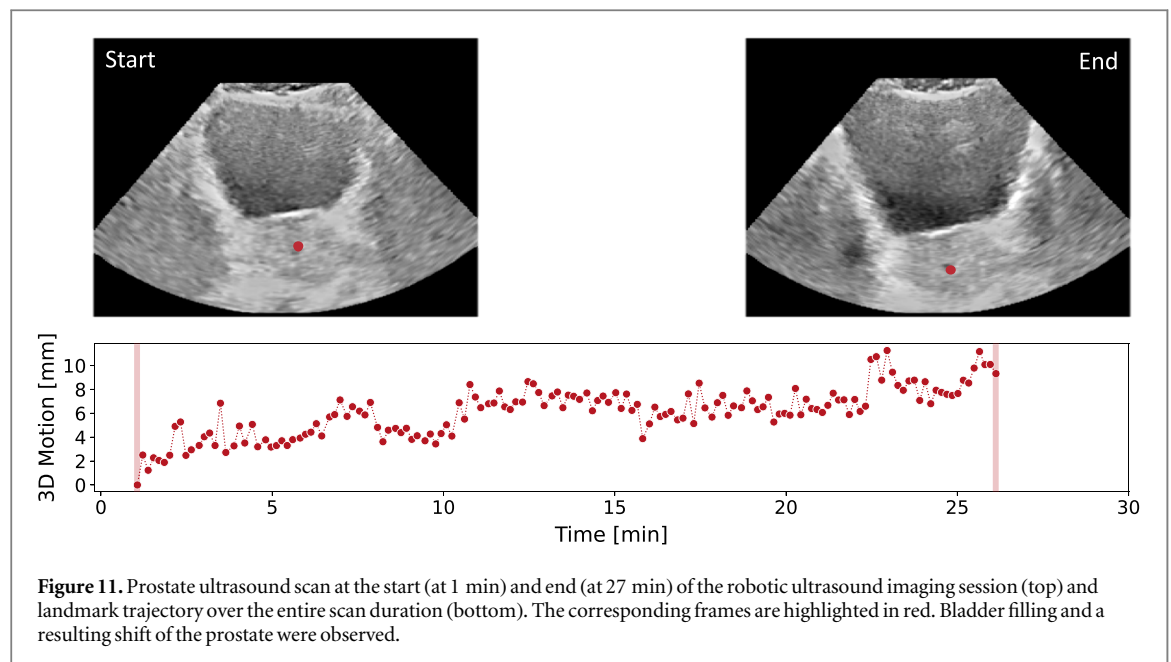


Figure 11. Prostate ultrasound scan at the start (at 1 min) and end (at 27 min) of the robotic ultrasound imaging session (top) and landmark trajectory over the entire scan duration (bottom). The corresponding frames are highlighted in red. Bladder filling and a resulting shift of the prostate were observed.

of rib shadows and thus a loss of anatomical information. These artefacts generally occurred in a small number of frames (0.1%) except for V2 where rib shadows appeared more frequently (1% of frames). In the prostate, abrupt changes in entropy values were observed in two volunteers (V4, V5) for 0.1% and 0.2% of frames and were likely caused by imaging artefacts from passing air or muscle contractions. The artefacts disappeared quickly without the need for manual probe repositioning.

None of the scanned individuals reported pain (mean score 4.0, scale 0–4) or discomfort (mean score 3.0) during robotic scan acquisition and probe pressure was considered acceptable.

Internal target motion

Motion results for the internal landmarks in liver and prostate are summarized in table 2. Figure 9 shows the annotated landmark locations at a liver vessel bifurcation and in the centroid of the prostate, respectively. Landmark positions were transformed into the robot reference frame to relate target motion to the main patient axes SI, AP and LR for better comprehensiveness of the results and their comparability with previous studies. The magnitude of landmark motion over time for all volunteers, relative to the starting position, is also illustrated in figure 9.

Liver

In contrast to the external probe motion results, the vessel bifurcations chosen as landmarks in the liver mainly followed periodic breathing patterns and only experienced a small number of isolated events with abrupt excursions. Figure 9 shows that motion patterns varied considerably among volunteers, with high-amplitude periodic motion (V2, V5) as well as abrupt target shifts but relatively low periodic amplitude changes (V1, V3, V4). Maximum target motion magnitudes were between 23.9 and 45.2 mm and interquartile ranges from 4.3 to 19.6 mm were observed. The individual motion components in all three axes are shown in figure 10 for one example trajectory (V3). For all volunteers, liver target motion was most pronounced in the SI direction, followed by AP and LR.

When comparing the median landmark positions measured in the beginning and the end of the scan acquisition (first and last 30 s), differences between 2.5 and 7.0 mm were observed. This implies a drift in landmark positions over time, albeit without a clear directionality among volunteers (see figure 9). The distance of the landmarks relative to their starting position in the first frame was over 3 mm for over 90% of the time (median, range 80%–97%). Excursions over 5 mm were observed for almost 75% of the time (range 48%–86%).

To investigate short-term motion patterns, two intervals of 30 s duration with a higher density of annotated frames were analysed for each scan session. An example for such a densely annotated interval is shown in figure 10. Target motion in these intervals varied between subjects, with a maximum motion extent of 13.8–44.9 mm and an interquartile motion range between 4.9 and 19.4 mm. For three of the five volunteers, the intra-subject differences in motion range between the two intervals were <1 mm, but 5 and 9 mm for the remaining two, indicating a considerable change in breathing patterns over time.

Prostate

Prostate motion showed lower magnitudes and less inter-subject variability compared to the liver (see figure 9). Maximum positional changes, measured over the entire scan time, ranged from 10.7 to 23.9 mm and interquartile ranges were between 1.8 and 4.7 mm, with no clear trend in directionality among subjects. Pronounced, abrupt target shifts were rare, isolated events which appeared in three out of five volunteers with magnitudes between 7.3 and 13.2 mm. They were caused by involuntary muscle contractions or voluntary pose adjustments of the volunteers.

Additionally, long-term drift of the landmark positions between the beginning and the end of the scan acquisitions were observed. A comparison of the median positions in the first and the last 30 s revealed drift magnitudes from 3.2 mm up to 9.9 mm. Those volunteers with the highest motion ranges tended to also show the strongest drift over time (e.g. V2, see figure 9). This slow drift of the prostate was likely caused by the expanding bladder volume due to the drinking protocol used for the prostate scans (see Methods section 2.3). An example of the prostate drifting over the 30 min scan period and the corresponding slice views through the ultrasound volumes are shown in figure 11. Prostate excursions relative to the starting position over 3 mm and 5 mm varied considerably between volunteers and were observed for 11%–93% and 1%–72% of the time, respectively.

Analysis of the two short-term intervals with annotations in every second frame revealed maximum and interquartile landmark motion ranges of 3.6 mm to 10.6 mm and 1.0 mm to 2.6 mm, respectively, with only minor intra-subject differences (< 1 mm) between first and second phase. Landmark motion in a short-term interval is illustrated in figure 10.

Discussion

The goal of this study was the stable acquisition of 4D ultrasound image data over extended scan sessions *in vivo*. Using robotic probe manipulation with active motion compensation, it was possible to continuously acquire 4D ultrasound in the liver and prostate of five healthy volunteers during free breathing without physical restraints or instructions over 30 min duration. To compensate for slow target shifts or imaging artefacts such as bone shadows in the ultrasound image data during scan acquisition, the probe position could be changed in real-time via force-sensitive remote control of the robot.

The desired target force of 10 N along the longitudinal probe axis was maintained within a narrow interquartile range of $\pm 1\%$ throughout the experiments. Despite short maximum forces of up to 21 N, none of the volunteers reported discomfort during scan acquisition and the maximum force threshold of 25 N was never exceeded. Previous studies on robotic ultrasound systems using force control approaches for motion compensation reported low errors and standard deviations comparable to the current study. Lediju Bell *et al* measured force control errors between 0.4 and 0.6 N for a force range from 2.5 to 25 N in three volunteers and low standard deviations between 0.1 and 1.3 N in a canine study using their custom-built robot (Lediju Bell *et al* 2014, 2016). An average error of 0.2 N was reported in Virga *et al* (2016) and a standard deviation of 0.9 N in Seitz *et al* (2020), demonstrating the high accuracy achievable with force control using the *LBR iiwa* robot confirmed by the current study.

While these results align well with previous studies on robotic force control for ultrasound imaging, it should be noted that the force values provided by the robot control software were not directly measured using force sensors but represent the result of internal calculations based on the current joint torques and a computational model defined by the manufacturer. Prior experiments have shown the possibility of errors occurring in these calculations, leading to the estimation of inaccurate force values (Kuhlemann 2019). This is especially likely for small forces and in robot configurations that approach singularities and joint limits. Caution should therefore be taken during setup and simulation to ensure reliable robot operation within the expected motion range.

The selected target force of 10 N in this study was chosen based on literature values and preliminary tests as a trade-off between robustness, image quality and patient comfort. It is important to note that contact forces reported for manual ultrasound scan acquisitions can show high variability, primarily depending on the patient's body mass index (BMI). For obese patients, probe contact force applied by the sonographer can be up to 270 N to reach sufficient image quality (Rousseau *et al* 2013). Force measurements during abdominal exams showed mean contact forces of 8.2 ± 4.3 N, with subjects of BMI > 25 requiring higher mean (10.5 N) and maximum (25.3 N) forces compared to subjects with lower BMI (mean 7.9 N, max 17.4 N) (Dhyani *et al* 2017). Additionally, robotic target forces in the literature vary depending on the clinical application scenario. Mean contact force values ranged from 3.2 N (Schlosser *et al* 2010) to 10.5 N (Lediju Bell *et al* 2014) for prostate scans during radiotherapy, and from 5.0 N (Seitz *et al* 2020) to 37.1 N (Lediju Bell *et al* 2014) for the liver. In Virga *et al* (2016), a mean contact force of 14.8 N was used for abdominal screening procedures while spinal scans were acquired with 5 N in Zettinig *et al* (2016) and 10 N in Esteban *et al* (2018). Considering these variations in contact

force based on patient body type and scanning site, an optimal target force for all robotic ultrasound exams cannot be defined. Among the ten datasets acquired in this study, differences in force distributions could be observed between target regions (liver versus prostate) and between individual subjects. While the five subjects included in this study had similar body types well-suited for sonography exams, it can be expected that differences in required forces will be even more pronounced in a larger, more diverse cohort. A solution to this problem could be the estimation of individualized force profiles for different patients and scan sites, for example by using an online adaptive force estimation based on confidence values calculated from the ultrasound image data as proposed in Virga *et al* (2016). Future work will focus on the design of suitable calibration approaches and classification strategies and the impact of applied contact pressure on image quality. A first indicator of this relation was already observed in this study where a correlation between entropy and contact force was measured.

Superficial probe motion controlled by the robot followed periodic sinusoidal patterns characteristic of breathing motion and was below 2 mm most of the time, with extreme shifts reaching over 10 mm in five out of ten scan sessions. Fast shifts of the body surface by several millimetres, for example due to coughing or other involuntary or voluntary movements of the volunteers, were successfully compensated by the developed system. Despite these events, probe contact was maintained continuously, resulting in unimpaired ultrasound image acquisition over the entire scan duration. This was confirmed by the high average entropy values and low standard deviations over time, calculated for each ultrasound volume as an indicator of image quality. Distinct entropy decreases were only observed at the scan start before contact was established and for volumes affected by shadowing artefacts. The amount of robotic probe motion required for motion compensation during long-term image acquisition differed between anatomical regions. As expected, the intercostal viewport for liver visualization was affected by pronounced surface motion of over 1 cm magnitude due to periodic breathing motion and shifts of the scanned person or the ultrasound probe during scan acquisition. Target shifts were followed by correcting the probe position via remote control of the robot in order to restore target visibility, for example to compensate for rib shadows that moved into the field of view, in four out of five liver scan sessions. These positional corrections caused probe shifts of several millimetres and were only seen in the liver. The transabdominal probe position chosen for the prostate showed lower average motion magnitudes with a predominant component in AP direction. Due to the extreme drinking protocol, it could be observed that the volunteers were growing more uneasy towards the end of the prostate scan sessions, contributing to higher motion magnitudes especially in the final minutes of the acquisition.

Liver motion in this study showed maximum magnitudes of over 40 mm and interquartile ranges from 4 mm up to almost 20 mm, with the main component in SI direction. The pronounced periodic motion patterns and the inter- and intra-subject variability are in accordance with previous studies on liver motion during free breathing, with detailed overviews for example in Korreman (2012), O'Shea *et al* (2016). In a similar study to observe long-term organ motion, Siebenthal *et al* acquired several 4D MRI scans over a one-hour period in their study on liver motion and found gradual organ drift of several millimetres as well as an inhomogeneous distribution of motion magnitudes of up to 20 mm throughout the liver (Von Siebenthal *et al* 2007). Other studies measured similar trends in liver motion over entire radiotherapy treatment sessions but were relying on monitoring surrogate signals such as electromagnetic transponders (Worm *et al* 2018) or external optical markers combined with implanted fiducials and correlation models (Liang *et al* 2018, Zhang *et al* 2020).

Landmarks in the prostate had an interquartile motion range between 1.8 and 4.7 mm and slow drift over time of up to almost 10 mm, with excursions over 5 mm occurring in 13% of the time. Considering that the drinking protocol used in this study provoked relatively quick and extensive filling of the bladder, these numbers were expected to be higher in comparison to similar studies on prostate motion measured during realistic radiotherapy treatment sessions. Ng *et al* report 3D prostate displacements over 5 mm only in 2% of the time based on kV-imaging of implanted fiducial markers (Ng *et al* 2012). Sihono *et al* used a 4D ultrasound system for motion monitoring during therapy delivery and found that the percentage of prostate excursions over 2 mm increased with time, reaching almost 10% after 4 min scan time (Sihono *et al* 2018). Another study utilizing the same system measured mean 3D displacements of 0.7 ± 1.5 mm for scan times of 7–8 min (Han *et al* 2018). The mechanical probe used in these studies provided a volumetric framerate of 1–2 Hz and was locked in a transperineal position for imaging, limiting its applicability to quasi-static organs such as the prostate or potentially breath-hold scenarios as described in Vogel *et al* (2018).

In comparison to most prior studies, this is the first time that liver and prostate motion were continuously observed with 4D imaging over a 30 min period. This could only be achieved with robotic automation since human operators would eventually experience fatigue and discomfort during such extended acquisition times with ultrasound imaging. The demonstrated long-term 4D image acquisition holds high potential for therapy guidance of procedures usually monitored with other modalities such as x-ray imaging and could potentially generate new diagnostic possibilities by granting insights into dynamic physiological processes that could not be observed otherwise. As a first example, it was possible to observe the filling process of the bladder and the resulting shift of the prostate in the image data acquired in this study.

Target motion in the ultrasound image data was quantified based on manual landmark annotations by one trained observer. While the accuracy of the annotations was not explicitly analysed in this context, previous studies have shown inter- and intraobserver uncertainties for manually defined landmarks of 1–2 mm in ultrasound (De Luca *et al* 2018, van der Meer *et al* 2013). Considering the low velocity and amplitude of typical prostate motion, the median interquartile motion range of 1.4 mm observed during the 30 s intervals (with annotations in every second frame) in the prostate could provide an indicator of the amount of intra-observer variability in the current study. As our primary goal was assessing the performance of the robotic ultrasound imaging system *in vivo*, the development and evaluation of a robust tracking algorithm for motion extraction from the ultrasound images was not part of this study. However, concepts for dynamic target localisation in 4D ultrasound utilizing features or deep learning methodologies are currently under investigation and profit from the large amount of image data generated in this study (Wulff *et al* 2019, 2020).

While the motion analysis in the current study has been limited to the 3D translation of a single landmark, the availability of continuous 4D image data also facilitates the extraction of rotational motion components as well as the generation of entire deformation fields in future studies. The data generated in this study, especially with the simultaneous acquisition of probe contact force, the external probe motion during imaging and the landmark annotations, provide valuable insights into the amount of motion and variability to be expected during robotic ultrasound scanning and can be further used for detailed motion analyses or tracking studies such as (De Luca *et al* 2018).

It should be noted that the possibility of a slight misalignment between the patient axes (LR, SI, AP) and the robot base (x, y, z) cannot be excluded since the transformations between the coordinate systems of the robot, the ultrasound image data and the scanned subjects were not explicitly calibrated in this study. As a result, the motion magnitudes observed in the experiments might not perfectly represent target motion along the main anatomical axes. While this initial feasibility study did not require calibration to absolute coordinates, certain application scenarios of the robotic ultrasound system will depend on it. If motion monitoring in absolute coordinates is required for the desired task, for example for image guidance during radiotherapy, the robot's base coordinate system must be calibrated to the treatment room, for example using a geometric calibration method as described in Kuhlemann *et al* (2015), Şen *et al* (2017), Ipsen *et al* (2018), Von Haxthausen *et al* (2020). To achieve the highest possible accuracy, the fixed transformation between the probe and the ultrasound image coordinates should also be determined via hand-eye calibration since perfect alignment of the ultrasound images with the probe's external geometry (e.g. membrane's centre point, main axes) or its position inside the holding mechanism cannot be assumed. Many hand-eye calibration approaches for 2D and 3D ultrasound probes have been published to date, e.g. (Bergmeir *et al* 2009, Bø *et al* 2015, Esposito *et al* 2019), and are applicable to the robotic ultrasound calibration problem.

Knowledge of the transformations between the patient, the robot and the ultrasound image coordinates is also a prerequisite for full automation of the probe positioning process. Previous studies have shown the potential of using 3D patient scans acquired prior to treatment, e.g. with CT or MRI, to pre-calculate optimal probe positions for ultrasound imaging on the patient surface (Bruder *et al* 2011, Gong *et al* 2015, Schlosser *et al* 2016, Camps *et al* 2017). Our current efforts therefore investigate the combination of these positioning guides with the calibrated setup of the developed robotic ultrasound system for (semi-)autonomous placement of the probe. The ultimate goal is to steer the probe robotically based on the image content in the ultrasound data to optimize target visibility or image quality autonomously. The current study indicates that entropy could be a suitable measure for image quality in this context by potentially allowing differentiation between images affected by artefacts and images with high-quality anatomical information (Kuhlemann *et al* 2014). Future investigations will focus on this relation and its potential use for (semi-)automated image quality optimization. Preliminary studies could already demonstrate the feasibility of autonomously following the vascular structure in a phantom (von Haxthausen *et al* 2020) or generating a sweep of the spine in healthy volunteers (Hase *et al* 2020, Tirindelli *et al* 2020) using the ultrasound image information for robot control.

The results of this study show that stable, long-term robotic ultrasound scanning during free breathing is possible and internal organ motion can be monitored in real time, making this a promising system for motion compensation tasks, for example in radiotherapy. However, the future use of robotic ultrasound in image-guided radiotherapy would require full integration into the clinical workflow. This implies not only a geometric calibration to treatment room coordinates and accurate target localization in the ultrasound data but also relies on an accurate and reproducible setup in the treatment room and optimized positioning of the robotic hardware to ensure efficient therapy delivery. Robotic probe placement for patient setup in the treatment room can be supported by using precalculated probe positions based on tomographic image data of the patient (Schlosser *et al* 2016, Bruder *et al* 2011, Camps *et al* 2017) or by providing collaborative robotic guidance during probe positioning to ensure reproducible target deformation from contact pressure (Lediju Bell *et al* 2014, Şen *et al* 2017). Another aspect currently under investigation is the optimization of the robotic setup based on treatment planning simulations, incorporating the robot's kinematics and dynamic configuration changes into the

treatment planning process (Schlüter *et al* 2019a, 2019b). These aspects are essential for future integration of the developed robotic ultrasound system into a radiotherapy motion management framework and require further investigation.

One of the study's main limitations is the cohort of scanned subjects. Based on our focus on demonstrating the feasibility of safe, robust ultrasound image acquisition using robotic probe manipulation, a small sample of five healthy volunteers was included. To avoid anxiety during scan acquisition, these volunteers were experienced in the field of robotics. Regarding their physical condition, especially body weight, they could be considered ideal for ultrasound imaging. In the future, larger and more diverse cohorts will be recruited for application-specific studies to better reflect typical patients of the envisioned application.

Conclusion

This study demonstrates the feasibility of robotic control and motion compensation of an ultrasound probe under realistic conditions during free breathing. Robotic 4D ultrasound image acquisition with dynamic force control can be used for stable, continuous imaging of the liver and prostate and other regions affected by motion. Slow target shifts and imaging artefacts, for example caused by rib shadows or bowel gas, were successfully compensated in real-time via force control and remote control of the robot. The developed system facilitates long-term acquisition of 4D image data over extended imaging sessions for the first time and holds the potential to be used for therapy guidance as well as diagnostic tasks. The data generated in this study, including ultrasound volumes, robot motion and force data as well as landmark annotations, can be made available upon request for further studies on motion monitoring in ultrasound image data.

Acknowledgments

Parts of this work were supported by the German Federal Ministry of Education and Research (grant no. 13GW0228B) and the German Research Foundation (grants no. ER 817/1-1 and ER 817/1-2). The authors have confirmed that any identifiable participants in this study have given their consent for publication.

Conflict of interest statement

The authors report no conflict of interest.

ORCID iDs

Svenja Ipsen  <https://orcid.org/0000-0001-5723-2679>

Daniel Wulff  <https://orcid.org/0000-0001-8892-5371>

Floris Ernst  <https://orcid.org/0000-0002-0474-6673>

References

- Bergmeier C, Seitel M, Frank C, De Simone R, Meinzer H P and Wolf I 2009 Comparing calibration approaches for 3D ultrasound probes *Int. J. Comput. Assist. Radiol. Surg.* **4** 203–13
- Boda-Heggemann J *et al* 2008 Intrafraction motion of the prostate during an IMRT session: a fiducial-based 3D measurement with cone-beam CT *Radiat. Oncol.* **3** 37
- Boda-Heggemann J *et al* 2019 Ultrasound-based repositioning and real-time monitoring for abdominal SBRT in DIBH *Phys. Med.* **65** 46–52
- Bruder R, Ernst F, Stender B, Richter L and Schweikard A 2011 SU-D-220-02: optimal transducer position for 4D ultrasound guidance in cardiac IGRT *Med. Phys.* **38** 3390
- Bø L E, Hofstad E F, Lindseth F and Hernes T A N 2015 Versatile robotic probe calibration for position tracking in ultrasound imaging *Phys. Med. Biol.* **60** 3499–513
- Camps S M, Verhaegen F, Paiva Fonesca G, de With P H N and Fontanarosa D 2017 Automatic transperineal ultrasound probe positioning based on CT scan for image guided radiotherapy *Proc. SPIE. Med. Imag. Image-Guided Proce. Robot. Interv. and Model.* **10135** 101352X
- Chatelain P, Krupa A and Navab N 2017 Confidence-driven control of an ultrasound probe *IEEE Trans. Robot.* **33** 1410–24
- Dhyani M *et al* 2017 A pilot study to precisely quantify forces applied by sonographers while scanning: a step toward reducing ergonomic injury *Work* **58** 241–7
- De Luca V *et al* 2015 The 2014 liver ultrasound tracking benchmark *Phys. Med. Biol.* **60** 5571–99
- De Luca V *et al* 2018 Evaluation of 2D and 3D ultrasound tracking algorithms and impact on ultrasound-guided liver radiotherapy margins *Med. Phys.* **45** 4986–5003
- Esposito M *et al* 2019 Total variation regularization of pose signals with an application to 3D freehand ultrasound *IEEE Trans. Med. Imaging* **0062** 1–1
- Esteban J *et al* 2018 Robotic ultrasound-guided facet joint insertion *Int. J. Comput. Assist. Radiol. Surg.* **13** 895–904

- Evans K, Roll S and Baker J 2009 Work-related musculoskeletal disorders (WRMSD) among registered diagnostic medical sonographers and vascular technologists *J. Diagn. Med. Sonogr.* **25** 287–99
- Fast M F, O'Shea T P, Nill S, Oelfke U and Harris E J 2016 First evaluation of the feasibility of MLC tracking using ultrasound motion estimation *Med. Phys.* **43** 4628–33
- Fenster A, Bax J, Neshat H, Kakani N and Romagnoli C 2013 3D Ultrasound Imaging in Image-Guided Intervention *Advancements and Breakthroughs in Ultrasound Imaging*, ed G Gunaratne (Rijeka: InTech) pp 1–26
- Fontanarosa D, van der Meer S, Bamber J, Harris E, O'Shea T and Verhaegen F 2015 Review of ultrasound image guidance in external beam radiotherapy: I. Treatment planning and inter-fraction motion management *Phys. Med. Biol.* **60** R77–114
- Giuliani M et al 2020 User-centred design and evaluation of a tele-operated echocardiography robot *Health Technol.* **10** 649–65
- Gong R, Bruder R, Schweikard A, Schlosser J and Hristov D 2015 CARS 2015—Computer Assisted Radiology and Surgery Proceedings of the 29th International Congress and Exhibition Barcelona *Int J CARS* **10** 1–312
- Grimwood A et al 2018 *In vivo* validation of Elekta's Clarity autoscans for ultrasound-based intrafraction motion estimation of the prostate during radiation therapy *Int. J. Radiat. Oncol. Biol. Phys.* **102** 912–21
- Han B et al 2018 Evaluation of transperineal ultrasound imaging as a potential solution for target tracking during hypofractionated radiotherapy for prostate cancer *Radiat. Oncol.* **13** 151
- Harris E J, Miller N R, Bamber J C, Symonds-Taylor J R N and Evans P M 2011 The effect of object speed and direction on the performance of 3D speckle tracking using a 3D swept-volume ultrasound probe *Phys. Med. Biol.* **56** 7127–43
- Harrison G and Harris A 2015 Work-related musculoskeletal disorders in ultrasound: Can you reduce risk? *Ultrasound* **23** 224–30
- Hase H et al 2020 Ultrasound-guided robotic navigation with deep reinforcement learning *IEEE/RSJ Int. Conf. on Intelligent Robots and Systems (IROS)* pp 5534–41 <http://ras.papercept.net/images/temp/IROS/files/1907.pdf>
- Ipsen S et al 2017 Simultaneous acquisition of 4D ultrasound and wireless electromagnetic tracking for *in-vivo* accuracy validation *Curr. Dir. Biomed. Eng.* **3** 75–8
- Ipsen S, Bruder R, Kuhlemann I, Jauer P, Motisi L, Cremers F, Ernst F and Schweikard A 2018 A visual probe positioning tool for 4D ultrasound-guided radiotherapy *40th Annu Int Conf IEEE Eng Med Biol Soc. (EMBC)* **2018** 883–6
- Ipsen S, Bruder R, O'Brien R, Keall P J, Schweikard A and Poulsen P R 2016 Online 4D ultrasound guidance for real-time motion compensation by MLC tracking *Med. Phys.* **43** 5695–704
- Korremans S S 2012 Motion in radiotherapy: photon therapy *Phys. Med. Biol.* **57** R161–91
- Kuhlemann I 2019 Methods for quasi-static tasks with redundant manipulators—advances in kinematics dexterity and sensitivity University of Luebeck, Germany
- Kuhlemann I, Bruder R, Ernst F and Schweikard A 2014 WE-G-BRF-09: force- and image-adaptive strategies for robotised placement of 4D ultrasound probes *Med. Phys.* **41** 523
- Kuhlemann I, Jauer P, Schweikard A and Ernst F 2015 Patient localization for robotized ultrasound-guided radiation therapy *Imaging Comput Assist Radiat Ther ICART 2015, 18th Int. Conf. Med Image Comput Comput Interv—MICCAI'15* pp 105–12 <https://hal.archives-ouvertes.fr/hal-01264358/document>
- Kuhlemann I, Schweikard A, Jauer P and Ernst F 2016 Robust inverse kinematics by configuration control for redundant manipulators with seven DoF *2nd Int. Conf. Control Autom Robot ICCAR* **2016** 49–55
- Lachaine M and Falco T 2013 Intrafractional prostate motion management with the Clarity Autoscan system *Med. Phys. Int.* **1** 72–80
- Lediju Bell M A, Kumar S, Kuo L, Sen H T, Iordachita I and Kazanzides P 2016 Toward standardized acoustic radiation force (ARF)-Based ultrasound elasticity measurements with robotic force control *IEEE Trans. Biomed. Eng.* **63** 1517–24
- Lediju Bell M A, Sen H T, Iordachita I, Kazanzides P and Wong J 2014 *In vivo* reproducibility of robotic probe placement for a novel ultrasound-guided radiation therapy system *J. Med. Imaging Radiat. Sci.* **1** 025001
- Liang Z et al 2018 Evaluation of the intra- and interfractional tumor motion and variability by fiducial-based real-time tracking in liver stereotactic body radiation therapy *J. Appl. Clin. Med. Phys.* **19** 94–100
- Ng J A et al 2012 Kilovoltage intrafraction monitoring for prostate intensity modulated arc therapy: first clinical results *Int. J. Radiat. Oncol. Biol. Phys.* **84** e655–61
- O'Shea T, Bamber J, Fontanarosa D, van der Meer S, Verhaegen F and Harris E 2016 Review of ultrasound image guidance in external beam radiotherapy part II: intra-fraction motion management and novel applications *Phys. Med. Biol.* **61** R90–137
- Priester A M, Natarajan S and Culjat M 2013 Robotic ultrasound systems in medicine *IEEE Trans. Ultrason. Ferroelectr. Freq. Control* **60** 507–23
- Rousseau T, Mottet N, Mace G, Franceschini C and Sagot P 2013 Practice guidelines for prevention of musculoskeletal disorders *J. Ultrasound Med.* **32** 157–64
- Schlosser J et al 2016 Robotic intrafractional US guidance for liver SABR: system design, beam avoidance, and clinical imaging *Med. Phys.* **43** 5951–63
- Schlosser J, Salisbury K and Hristov D 2010 Telerobotic system concept for real-time soft-tissue imaging during radiotherapy beam delivery *Med. Phys.* **37** 6357–67
- Schlosser J, Salisbury K and Hristov D 2010 Evaluation of a telerobotic system concept for real-time soft-tissue image guidance during radiotherapy delivery *Int. J. Radiat. Oncol. Biol. Phys.* **78** S41
- Schlüter M, Fürweger C and Schläefer A 2019a Optimizing robot motion for robotic ultrasound-guided radiation therapy *Phys. Med. Biol.* **64** 195012
- Schlüter M, Gerlach S, Fürweger C and Schläefer A 2019b Analysis and optimization of the robot setup for robotic-ultrasound-guided radiation therapy *Int. J. Comput. Assist. Radiol. Surg.* **14** 1379–87
- Seitz P K, Baumann B, Johnen W, Lissek C, Seidel J and Bendl R 2020 Development of a robot-assisted ultrasound-guided radiation therapy (USgRT) *Int. J. Comput. Assist. Radiol. Surg.* **15** 491–501
- Swerdlow D R, Cleary K, Wilson E, Azizi-Koutenaei B and Monfaredi R 2017 Robotic arm-assisted sonography: review of technical developments and potential clinical applications *Am. J. Roentgenol.* **208** 733–8
- Sihono D S K et al 2018 Determination of intrafraction prostate motion during external beam radiation therapy with a transperineal 4-Dimensional ultrasound real-time tracking system *Int. J. Radiat. Oncol. Biol. Phys.* **101** 136–43
- Şen H T et al 2016 Cooperative control with ultrasound guidance for radiation therapy *Front. Robot. AI* **3** 1–12
- Şen H T et al 2017 System integration and *in vivo* testing of a robot for ultrasound guidance and monitoring during radiotherapy *IEEE Trans. Biomed. Eng.* **64** 1608–18
- Şen H T, Bell M A L, Iordachita I, Wong J and Kazanzides P 2013 A cooperatively controlled robot for ultrasound monitoring of radiation therapy *2013 IEEE Int. Conf. Intell Robot Syst IROS* **2013** 3071–6

- Tirindelli M *et al* 2020 Force-ultrasound fusion: bringing spine robotic-US to the next 'Level.' 2020 *IEEE/RSJ Int. Conf. on Intelligent Robots and Systems (IROS) (Las Vegas, NV, USA (virtual))*
- Von Haxthausen F, Böttger S, Wulff D, Hagenah J, García-Vázquez V and Ipsen S 2021 Medical robotics for ultrasound imaging: current systems and future trends *Curr. Robot. Rep.* **2** 55–71
- von Haxthausen F, Hagenah J, Kaschwich M, Kleemann M, García-Vázquez V and Ernst F 2020 Robotized ultrasound imaging of the peripheral arteries—a phantom study *Curr. Dir. Biomed. Eng.* **6** 20200033
- Von Haxthausen F, Ipsen S, Schwegmann H, Bruder R, Ernst F and García-Vázquez V 2020 A 3D Slicer module for calibration of spatially tracked 3D ultrasound probes *Proc. of CARS 2020; Int. J. Comput. Assist. Radiol. Surg.* **15** 1–214
- van der Meer S *et al* 2013 Critical assessment of intramodality 3D ultrasound imaging for prostate IGRT compared to fiducial markers *Med. Phys.* **40** 071707
- Von Siebenthal M, Székely G, Lomax A J and Cattin P C 2007 Systematic errors in respiratory gating due to intrafraction deformations of the liver *Med. Phys.* **34** 3620–9
- Virga S, Zettinig O, Esposito M, Pfister K, Frisch B, Neff T, Navab N and Hennemersperger C 2016 Automatic force-compliant robotic Ultrasound screening of abdominal aortic aneurysms *IEEE Int. Conf. Intell Robot Syst. 2016* **2016** 508–13
- Virga S, Göbl R, Baust M, Navab N and Hennemersperger C 2018 Use the force: deformation correction in robotic 3D ultrasound *Int. J. Comput. Assist. Radiol. Surg.* **13** 619–27
- Vogel L *et al* 2018 Intra-breath-hold residual motion of image-guided DIBH liver-SBRT: an estimation by ultrasound-based monitoring correlated with diaphragm position in CBCT *Radiother. Oncol.* **129** 441–8
- Wang S *et al* 2019 Robotic-assisted ultrasound for fetal imaging: evolution from single-arm to dual-arm system *Towards Auto. Rob. Syst. TAROS 2019 (Lecture Notes in Computer Science)* 11650 (Cham: Springer) pp 27–38
- Worm E S *et al* 2018 A prospective cohort study of gated stereotactic liver radiation therapy using continuous internal electromagnetic motion monitoring *Int. J. Radiat. Oncol. Biol. Phys.* **101** 366–75
- Wulff D, Hagenah J, Ipsen S and Ernst F 2020 Learning local feature descriptions in 3D ultrasound *20th IEEE Int. Conf. on BioInformatics and BioEngineering (BIBE) (Piscataway, NJ: IEEE)* pp 323–30 Virtual
- Wulff D, Kuhlemann I, Ernst F, Schweikard A and Ipsen S 2019 Robust motion tracking of deformable targets in the liver using binary feature libraries in 4D ultrasound *Curr. Dir. Biomed. Eng.* **5** 601–4
- Zettinig O, Fuerst B, Kojcev R, Esposito M, Salehi M and Wein W 2016 Toward real-time 3D ultrasound registration-based visual servoing for interventional navigation *2016 IEEE Int. Conf. on Robotics and Automation, ICRA* **2016** 945–50
- Zhang J, Wang L, Li X, Huang M and Xu B 2020 Quantification of intrafraction and interfraction tumor motion amplitude and prediction error for different liver tumor trajectories in Cyberknife synchrony tracking *Int. J. Radiat. Oncol.* **109** 1588–605